QM Final

Hung-Yu Wang

B10202052, NTU Physics

December 28, 2022

1-(a)

Theory

The Dirac equation

This derivation is adapted a little from [1], we write down the Dirac equation under electromagnetic interactions

$$\begin{bmatrix} m & \sigma\cdot\tilde{\mathbf{p}} \\ \sigma\cdot\tilde{\mathbf{p}} & -m \end{bmatrix}\begin{bmatrix} u \\ v \end{bmatrix} = E\begin{bmatrix} u \\ v \end{bmatrix} \quad \text{where} \quad \Psi = \begin{bmatrix} u \\ v \end{bmatrix}, \quad \tilde{\mathbf{p}} \equiv \mathbf{p} - e\mathbf{A} \tag{1}$$

Let $E = K + m$ and consider nonrelativistic case such that $K \ll m$. The second equation becomes

$$\sigma\cdot\tilde{\mathbf{p}}u - mv = (K+m)v \implies \sigma\cdot\tilde{\mathbf{p}}u \approx 2mv \tag{2}$$

And lets us write the first equation

$$mu + \sigma\cdot\tilde{\mathbf{p}}v = (K+m)u \implies \sigma\cdot\tilde{\mathbf{p}}v = Ku \tag{3}$$

substitute $\sigma\cdot\tilde{\mathbf{p}}u = 2mv$ and use the identity

$$(\sigma\cdot\mathbf{a})(\sigma\cdot\mathbf{b}) = \mathbf{a}\cdot\mathbf{b} + i\sigma\cdot(\mathbf{a}\times\mathbf{b}) \tag{4}$$

$$\implies \frac{(\sigma\cdot\tilde{\mathbf{p}})(\sigma\cdot\tilde{\mathbf{p}})}{2m}u = \left[\frac{\tilde{p}^2}{2m} + \frac{i\sigma}{2m}\cdot(\tilde{\mathbf{p}}\times\tilde{\mathbf{p}})\right]u = Ku \tag{5}$$

Recall $\tilde{\mathbf{p}} = \mathbf{p} - e\mathbf{A}$

$$\tilde{\mathbf{p}}\times\tilde{\mathbf{p}}u = (i\boldsymbol{\nabla} + e\mathbf{A})\times(i\boldsymbol{\nabla}u + e\mathbf{A}u) \tag{6}$$

$$= ie[\boldsymbol{\nabla}\times(\mathbf{A}u) + \mathbf{A}\times\boldsymbol{\nabla}u] = ie\mathbf{B}u \tag{7}$$

Then put it into equation (5)

$$\frac{\tilde{p}^2}{2m}u + \frac{i\sigma}{2m}\cdot(ie\mathbf{B})u = Ku \tag{8}$$

Since the interaction energy of a magnetic dipole is $-\mu\cdot\mathbf{B}$, therefore

$$\mu = \frac{\sigma e}{2m} = g\frac{e}{2m}\mathbf{S}, \quad \mathbf{S} = \frac{\hbar}{2}\sigma \implies g = 2 \tag{9}$$

Anomalous magnetic dipole moment and Standard model

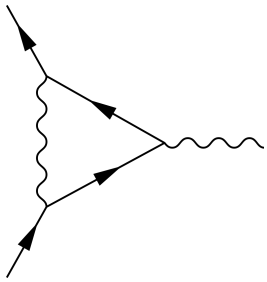

Figure 1: One-loop correction to a fermion's magnetic dipole moment.

The anomalous term $a \equiv \frac{g-2}{2}$. There are different calculation in history. The dirac equation imply $a = 0$. However by calculating the vertex function of one-loop diagram(Figure 1), we can get $a = \frac{\alpha}{2\pi}$, where α is the fine-structure constant. This result was given by Julian Schwinger in 1948 [7]

Nowadays, Standard model predict that

$$\frac{g}{2} = 1 + a_{\text{QED}} + a_{\text{hadronic}} + a_{\text{weak}} \tag{10}$$

Quantum electrodynamics gives a_{QED} as a power series in the fine-structure constant

$$a_{\text{QED}}(\alpha) = C_2(\frac{\alpha}{\pi}) + C_4(\frac{\alpha}{\pi})^2 + C_6(\frac{\alpha}{\pi})^3 + \dots \tag{11}$$

The contribution of a_{hadronic} just about two parts per trillion. And a_{weak} is smaller than the measurement precision.

In 1996, [3] gives the analytical value of coefficient C_6. And [5] gets the numerical value up to α^5. Finally

$$a(\text{theory}) = 1,159,652,181.643(25)(23)(16)(763) \times 10^{-12} \tag{12}$$

This value comes from the evaluation of the electron anomalous magnetic moment a_e which arises from a gauge-invariant set, called Set V, consisting of 6354 tenth-order Feynman diagrams without closed lepton loops.

It's the improvement of [8]. The number in parentheses is worth to talk about. The first three uncertainties are from the eighth-order, tenth-order, and hadronic and elecroweak terms. The fourth and largest uncertainty is from α, the fine-structure constant derived from the rubidium recoil measurement.

Conclusion

Standard model predict an astonishing precisely number of a, which has 13 significant digits. Everything is waiting for the experimental verification.

Experiment

Measurement of g

I will show how $g/2 = 1.001\,159\,652\,180\,73(28)$ be measured. The measurement is done by Hanneke group in 2008 [6].

The key elements are

1. Quamtum jump spectroscopy and Quantum non-demolition (QND) measurements: The transition frequency can be used to calculate cyclotron frequency.
2. Inhibited spontaneous emission: The radiative decay of the cyclotron motion of a single electron is significantly inhibited when the electron is located within a microwave cavity (formed by the electrodes of a Penning trap) rather than in free space. [11]
3. A one-particle self-excited oscillator(SEO): It helps us to understand the interaction between electron and cavity.
4. Low Temperature: To keep the cyclotron motion in its quantum ground state.
5. Cyclotron motion: It's stable and easy to understand by superposition principal .

A cylindrical Penning trap cavity

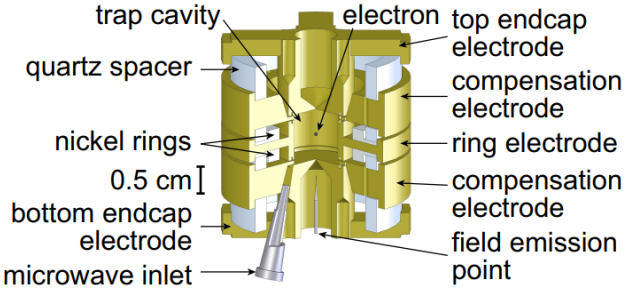

Figure 2: Cylindrical Penning trap cavity used to confine a single electron and inhibit spontaneous emission.

The rings and cap are the SEO system (figure 3). The cyclotron drive is microwave radiation injected into the trap cavity through a cold attenuator to keep black body photons from entering the trap. The electrode and field emission point is the source of electric field and magnetic field.

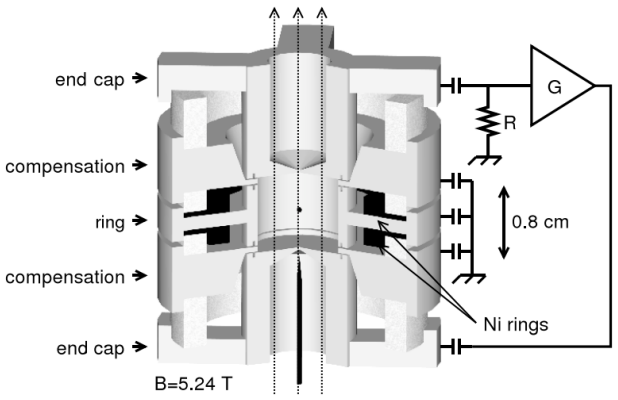

Figure 3: The vertical oscillation of a trapped electron, shown within a cutaway of a cylindrical Penning trap, induces a voltage across resistor R that is amplified and fed back to drive the oscillation. Unavoidable trap capacitance in parallel to R is tuned out at !z with a parallel inductor. [10]

The importance of temperature

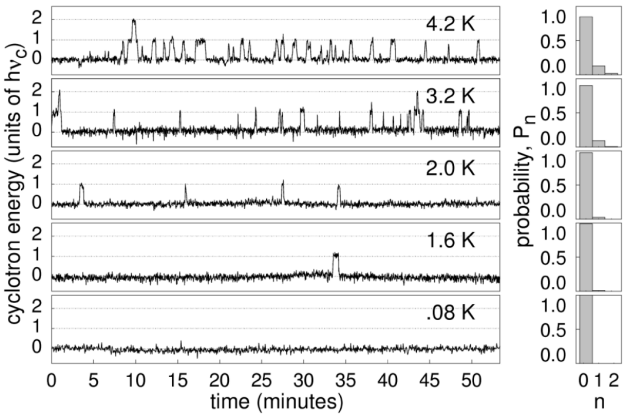

Figure 4: Quantum jumps between the lowest states of the one electron cyclotron oscillator decrease in frequency as the cavity temperature is lowered. [9]

As figure 4 show that **temperature** is critical parameter. When the cavity temperature less than 80mK, the cyclotron stays in its ground state until a resonant photon is injected.

Purpose and calculation

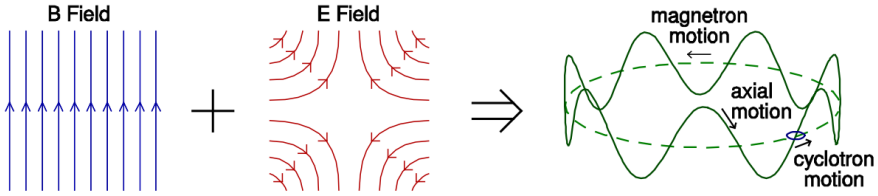

motion	frequency	$h\upsilon/k_B$	damping
axial	200 MHz	9.6 mK	1 Hz
cyclotron	149.0 GHz	7.2 K	0.02 Hz
spin	149.2 GHz	7.2 K	10^{-12} Hz
magnetron	130 kHz	6.4 μK	10^{-17} Hz

Figure 5: The configuration of cyclotron. (This figure comes from Brain Odom, Harvard University, Gabrielse group)

Use the definition of **electron g-factor**, the property of cyclotron frequency $\omega_c = eB/m$ and the spin frequency is proportional to magnetic field $\omega_s = -\dfrac{2\mu B}{\hbar}$

$$\frac{g}{2} = -\frac{\mu}{\mu_B} = \frac{\omega_s}{\omega_c} = \frac{\omega_c + \omega_a}{\omega_c}, \quad \text{where} \quad \omega_a \equiv \omega_s - \omega_c \tag{13}$$

Above is the case without **E**, by some generalization(Brown-Gabrielse invariance theorem), we can arrive at this equation to fit the experiment:

$$\frac{g}{2} \approx 1 + \frac{\bar{\nu}_a - \bar{\nu}_z^2/(2\bar{f}_c)}{\bar{f}_c + 3\delta/2 + \bar{\nu}_z^2/(2\bar{f}_c)} + \frac{\Delta g_{\text{cav}}}{2} \tag{14}$$

where $\bar{f}_c \equiv \nu_v - 3\delta/2$ is cyclotron frequency, anomaly transition frequency $\bar{\nu}_a$, relativistic shift $\delta/\nu_c \equiv h\nu_c/(mc^2)$, axial frequency ν_z and cavity shift $\Delta g_{\text{cav}}/2$, seeing figure 6 for more information.

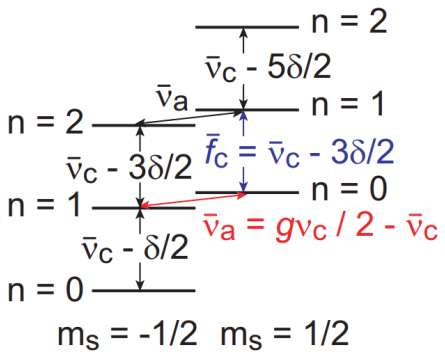

Figure 6: Electron's lowest cyclotron and spin levels.

Since the two frequencies can be measured to high precision, the cavity shifts become a major uncertainty. Better measurement and understanding of the electron-cavity interaction removes it. The author [6] using the electron itself to determine the cavity-electron interaction. The method [10] called self-excited oscillator (SEO), which can detect small frequency shifts quickly.

Remove the uncertainty of cavity shift, put the measured number in and do some statistical analysis, we finally get

$$\frac{g}{2} = 1.001\,159\,652\,180\,73(28) \tag{15}$$

Measurement of fine-structure constant

The atom recoil methods utilize measurements of transition frequencies and mass ratios, as well as either a Rb recoil velocity (in an optical lattice).[12] The fine structure constant is related to the ratio h/m_X for atom X by this equation from [13]

$$\alpha^2 = \frac{2R_\infty}{c}\frac{A_r(X)}{A_r(e)}\frac{h}{m_X} \tag{16}$$

where several terms are known with a very small uncertainty: R_∞ the Rydberg constant, $A_r(e)$ the electron relative mass and $A_r(\mathrm{Rb})$ the Rb relative mass with uncertainty less than 2.0×10^{-10}.

The fine structure constant α deduced from the measurement of the ratio h/m_{Rb} based on Bloch oscillations.

The result [12] gives $\alpha^{-1} = 137.035\,998\,78(91)$.

Conclusion

$$\text{Predicted}: \frac{g}{2} = -\frac{\mu}{\mu_B} = 1.001\,159\,652\,181\,643(25) \tag{17}$$

$$\text{Measured}: \frac{g}{2} = -\frac{\mu}{\mu_B} = 1.001\,159\,652\,180\,73(28) \tag{18}$$

The standard model is the great success and the great frustration of modern physics. It does predict the electron magnetic moment to a part per trillion. That's amazing.

1-(b)

The Muon $g-2$ Experiment

Physicists expect a new physics, one that goes beyond the standard model. Good news for them, the anomalous magnetic dipole moment of muon is so slightly more than theory predicts. That small anomaly just 2.5 parts in 1 billion. Such a small difference may seem irrelevant, but previous successes in electron have convinced physicists that there must be an unknown theory behind it.

Wrong theory? Or is it a calculation error?

Since 2017 more than 100 theoretical physicists have given a consensus value for the Standard Model predictions in a series of seminars. In 2020, they gave a hodgepodge of results.

Besides, some theorists believe that we can use "lattice QCD" technique to fit the experimental data.

The new data seems to stand in "lattice" method

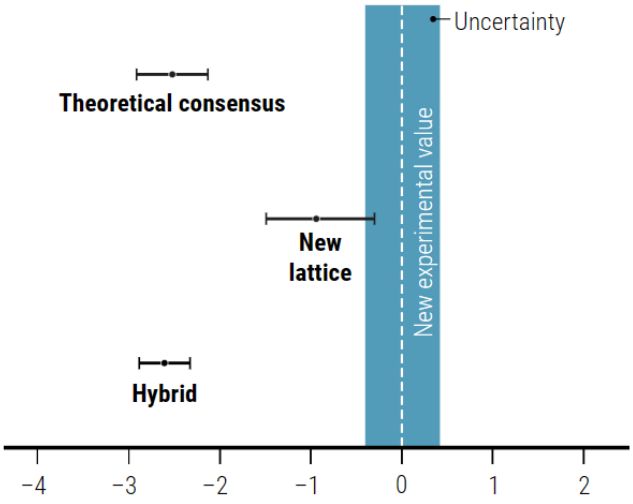

Figure 7: Difference between measured and theoretical values (parts per billion)

Some physicists think that the uncertainty of the consensus value calculated by the old method comes from the uncertainty of the input data, while the uncertainty of the lattice method comes from the reliability of the method itself, which is difficult to quantify and explain. Therefore, we shouldn't put so much effort into lattice calculations.

On the other hand, some physicists think that the standard model may be correct as before, since the new "lattice" value is closed the experimental result.

2

(a)

$$\mathbf{B} = \langle B_{\text{rf}} \cos(\omega t), -B_{\text{rf}} \sin(\omega t), B_0 \rangle \tag{19}$$

$$H = -\gamma \mathbf{B} \cdot \mathbf{S} = -\gamma \frac{\hbar}{2} \mathbf{B} \cdot \sigma = -\frac{\gamma \hbar}{2} \begin{pmatrix} B_0 & B_{\text{rf}} e^{i\omega t} \\ B_{\text{rf}} e^{-i\omega t} & -B_0 \end{pmatrix} \tag{20}$$

(b)

$i\hbar\dot{\chi} = H\chi$, $\omega_0 = \gamma B_0$ and $\Omega = \gamma B_{\text{rf}} \implies$

$$i\hbar \begin{pmatrix} \dot{a} \\ \dot{b} \end{pmatrix} = -\frac{\gamma\hbar}{2} \begin{pmatrix} B_0 & B_{\text{rf}} e^{i\omega t} \\ B_{\text{rf}} e^{-i\omega t} & -B_0 \end{pmatrix} \begin{pmatrix} a \\ b \end{pmatrix} = -\frac{\hbar}{2} \begin{pmatrix} \omega_0 & \Omega e^{i\omega t} \\ \Omega e^{-i\omega t} & -\omega_0 \end{pmatrix} \begin{pmatrix} a \\ b \end{pmatrix} \tag{21}$$

Expand it

$$\dot{a} = \frac{i}{2}(\Omega e^{i\omega t} b + \omega_0 a) \tag{22}$$

$$\dot{b} = \frac{i}{2}(\Omega e^{-i\omega t} a - \omega_0 b) \tag{23}$$

(c)

Use the method of separation variable $a = A(t)e^{i\omega t/2}, \quad b = B(t)e^{-i\omega t/2}$, Substitute into equation (22) & (23) and then express it

$$\begin{pmatrix} \dot{A} \\ \dot{B} \end{pmatrix} = \frac{i}{2} \begin{pmatrix} \omega_0 - \omega & \Omega \\ \Omega & \omega - \omega_0 \end{pmatrix} \begin{pmatrix} A \\ B \end{pmatrix} = \frac{i}{2} M \begin{pmatrix} A \\ B \end{pmatrix} \tag{24}$$

where M is a constant matrix. Now we diagonalize the matrix.

$$\begin{vmatrix} \omega_0 - \omega - \lambda & \Omega \\ \Omega & \omega - \omega_0 - \lambda \end{vmatrix} = 0 \implies \lambda = \pm\sqrt{(\omega - \omega_0)^2 + \Omega^2} = \omega' \tag{25}$$

Find the eigenvectors

$$\begin{pmatrix} \omega_0 - \omega - \omega' & \Omega \\ \Omega & \omega - \omega_0 - \omega' \end{pmatrix} \mathbf{v}_1 = 0 \implies \mathbf{v}_1 = \begin{pmatrix} \Omega \\ \omega - \omega_0 + \omega' \end{pmatrix} \tag{26}$$

$$\begin{pmatrix} \omega_0 - \omega + \omega' & \Omega \\ \Omega & \omega - \omega_0 + \omega' \end{pmatrix} \mathbf{v}_2 = 0 \implies \mathbf{v}_2 = \begin{pmatrix} \Omega \\ \omega - \omega_0 - \omega' \end{pmatrix} \tag{27}$$

Let $S = \begin{pmatrix} \mathbf{v}_1 & \mathbf{v}_2 \end{pmatrix}$ and fit the initial condition $a(0) = a_0\, b(0) = b_0$. The solution is

$$\begin{pmatrix} A \\ B \end{pmatrix} = e^{(i/2)Mt} \begin{pmatrix} a_0 \\ b_0 \end{pmatrix} = S \begin{pmatrix} e^{i\omega' t/2} & 0 \\ 0 & e^{-i\omega' t/2} \end{pmatrix} S^{-1} \begin{pmatrix} a_0 \\ b_0 \end{pmatrix} \tag{28}$$

Express it, then get

$$a(t) = \left[a_0 \cos\frac{\omega' t}{2} + \frac{i}{\omega'}\Big[a_0(\omega_0 - \omega) + b_0\Omega\Big] \sin\frac{\omega' t}{2} \right] e^{i\omega t/2} \tag{29}$$

$$b(t) = \left[b_0 \cos\frac{\omega' t}{2} + \frac{i}{\omega'}\Big[b_0(\omega_0 - \omega) + a_0\Omega\Big] \sin\frac{\omega' t}{2} \right] e^{-i\omega t/2} \tag{30}$$

(d)

For $a(0) = 1$, $b(0) = 0$, we have

$$b(t) = i\frac{\Omega}{\omega'} \sin\frac{\omega' t}{2} e^{-i\omega t/2} \implies P_{\text{down}}(t) = |b(t)|^2 = (\frac{\Omega}{\omega'})^2 \sin^2\frac{\omega' t}{2} \tag{31}$$

(e)

MRI

Introduction

The key idea is that our body is pretty much entirely made of water. So, we can receive the signal from hydrogen atoms by NMR. Since the process of NMR doesn't mess up any of the chemical properties of the tissues, so your body continues to function normally while the doctor makes the measurement. This advantage has made MRI a very popular medical research method.

The power of MRI

MRI is essentially an imaging technique that, like a telescope, has many parameters that can be adjusted and can have different color temperature for the same picture.

There is two different parameter called spin–lattice relaxation time and spin-spin relaxation time. Since the different physics property of them, the "photo" have two branch to imaging our body.

Signal	T1-weighted	T2-weighted
High	• Fat[17][18] • Subacute hemorrhage[18] • Melanin[18] • Protein-rich fluid[18] • Slowly flowing blood[18] • Paramagnetic or diamagnetic substances, such as gadolinium, manganese, copper[18] • Cortical pseudolaminar necrosis[18] • Anatomy	• More water content,[17] as in edema, tumor, infarction, inflammation and infection[18] • Extracellularly located methemoglobin in subacute hemorrhage[18] • Fat • Pathology
Inter-mediate	Gray matter darker than white matter[19]	White matter darker than grey matter[19]
Low	• Bone[17] • Urine • CSF • Air[17] • More water content,[17] as in edema, tumor, infarction, inflammation, infection, hyperacute or chronic hemorrhage[18] • Low proton density as in calcification[18]	• Bone[17] • Air[17] • Low proton density, as in calcification and fibrosis[18] • Paramagnetic material, such as deoxyhemoglobin, intracelullar methemoglobin, iron, ferritin, hemosiderin, melanin[18] • Protein-rich fluid[18]

Figure 8: The standard display of MRI images is to represent fluid characteristics in black and white images, where different tissues turn out as above. [14]

For example, these two imaging methods can distinguish gray matter from white matter in the brain.

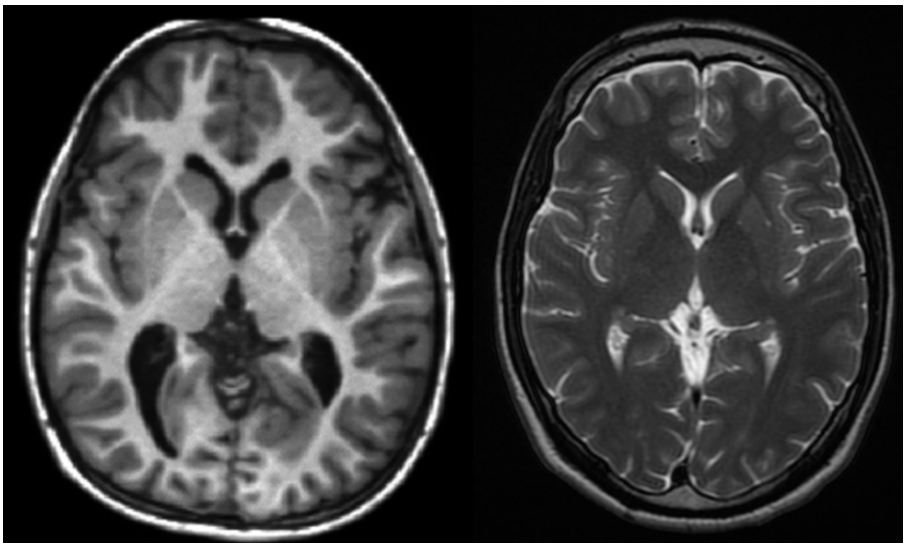

Figure 9: The left side is T1-weighted and the right side is T2-weighted. For T1, Gray matter darker than white matter, and vice versa.

Each tissue returns to its equilibrium state after excitation.

During nuclear magnetic resonance observations, spin–lattice relaxation is the mechanism by which the longitudinal component of the total nuclear magnetic moment vector (parallel to the

constant magnetic field) exponentially relaxes from a higher energy, non-equilibrium state to thermodynamic equilibrium with its surroundings (the "lattice"). It is characterized by the spin–lattice relaxation time, a time constant known as T1.

There is a different parameter, T2, the spin-spin relaxation time, which concerns the exponential relaxation of the transverse component of the nuclear magnetization vector (perpendicular to the external magnetic field). Measuring the variation of T1 and T2 in different materials is the basis for some magnetic resonance imaging techniques.[15]

Besides, T1 using a short repetition time (TR) and echo time (TE). T2 is measuring spin–spin relaxation by using long TR and TE times. Where Repetition Time (TR) is the amount of time between successive pulse sequences applied to the same slice. And, the echo time (TE) refers to the time between the application of the radiofrequency excitation pulse and the peak of the signal induced in the coil.

MRI recording: Real-time MRI

Real-time MRI refers to the continuous imaging of moving objects (such as the heart) in real time.

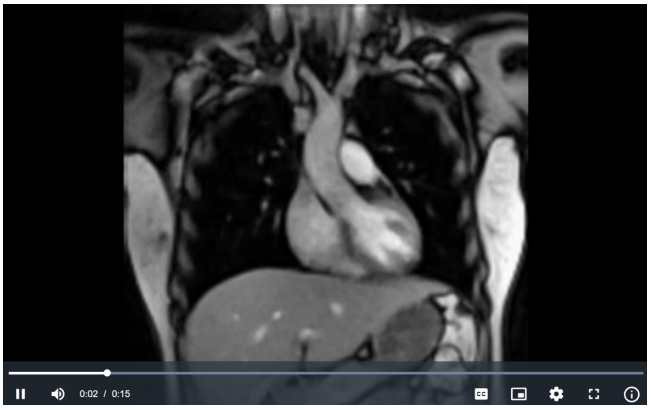

Figure 10: Heartbeat Video by real-time MRI [16]

Real-time MRI is likely to add important information on diseases of the heart and the joints, and in many cases may make MRI examinations easier and more comfortable for patients, especially for the patients who cannot hold their breathings or who have arrhythmia.

Magnetic resonance spectroscopy

Just as astronomers use spectrum to analyze distant stars, doctors can use MRS to understand the metabolites of the human body.

Magnetic resonance spectroscopy is an analytical technique that can be used to complement the more common magnetic resonance imaging (MRI) in the characterization of tissue.

The character of different metabolite often be the intensity of **Major Chemical Shift**

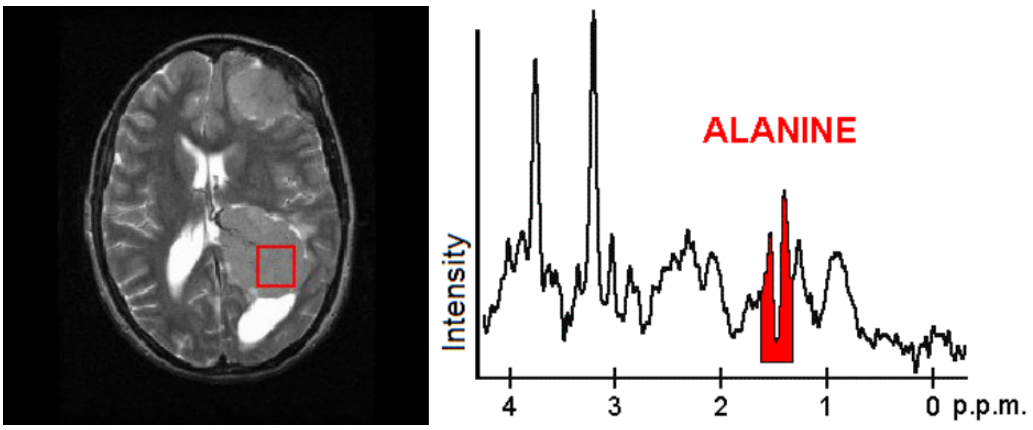

Figure 11: The peaks corresponding to the amino acid alanine, are highlighted in red (at 1.4 ppm chamical shift) This is an example of the kind of biochemical information which can help doctors to make their diagnosis. Other metabolites of note are choline (3.2 ppm) and creatine (3.0 ppm). [17]

MRS has uses not only in medicine but also in palaeontology.

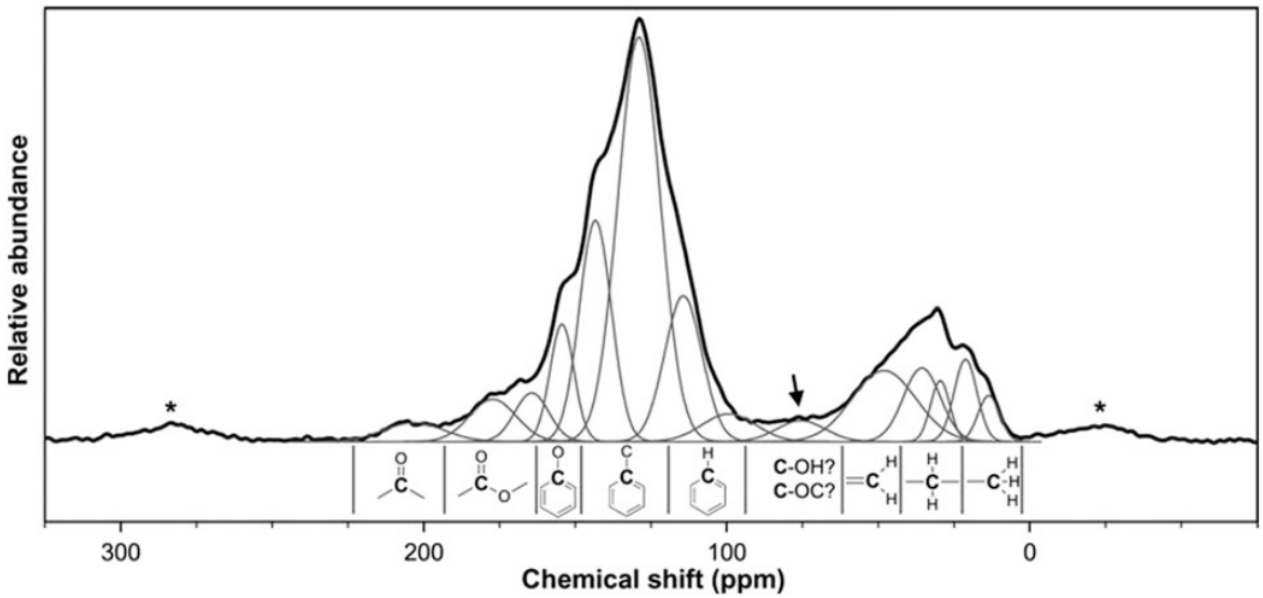

Figure 12: Representative ^{13}C NMR spectrum of fossil fern kerogen from Clarno chert (thick black line) and results of its deconvolution (gray lines) [19]

The light of MRI: Contrast agents and Multinuclear imaging

Hydrogen has the most frequently imaged nucleus in MRI because it is present in biological tissues in great abundance, and because its high gyromagnetic ratio gives a strong signal. However, any nucleus with a net nuclear spin could potentially be imaged with MRI. For example, **Helium-3, which is air.**

Helium-3 nuclei have an intrinsic nuclear spin of 1/2, and a relatively high magnetogyric ratio. Following inhalation, gas mixtures containing the hyperpolarized helium-3 gas can be imaged with an MRI scanner to produce anatomical and functional images of lung ventilation. This technique is also able to produce images of the airway tree, locate unventilated defects, measure the alveolar oxygen partial pressure, and measure the ventilation/perfusion ratio.

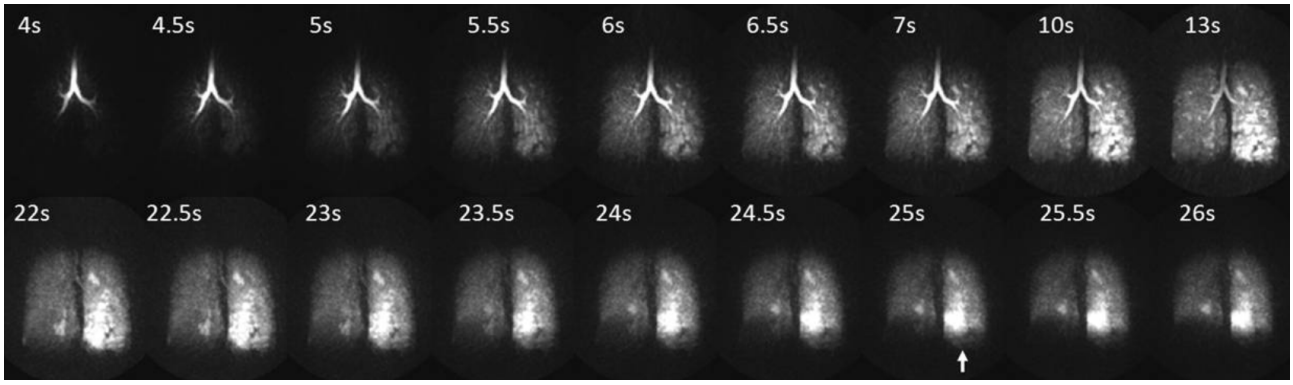

Figure 13: Using hyperpolarized He-MRI to assess ventilation and gas trapping using a forced exhalation maneuver in asthma. [18]

It is important to note that He-MRI is unique among pulmonary imaging methods because of its high spatial and temporal resolution of respiratory disease morphology (ADC) and function (ventilation volumetry) and its safe use across a wide variety of vulnerable pediatric, respiratory compromised and elderly patients (25) to explore mechanisms of disease pathophysiology.

3 Anyon

Introduction

In three-dimensions, bosons are symmetric under exchange and fermions are anti-symmetric under exchange. However, in two-dimensions, it is possible to have particles that are neither anti-symmetric nor symmetric under exchange. These particles are known as anyons. It has been shown that the exotic statistics of anyons can be used to encode information for topological quantum computation, and it is believed that they can be used in the construction of superconductors. [20]

Identical particles evolving in a three dimensional space

Let us consider a wave function $\psi(1,2)$ describing two identical particles. Apply an operator rotating particle 2 around particle 1 by an angle $\Delta\phi$

$$\psi(1,2) \to \psi'(1,2) = e^{i\nu\Delta\phi}\psi(1,2) \tag{32}$$

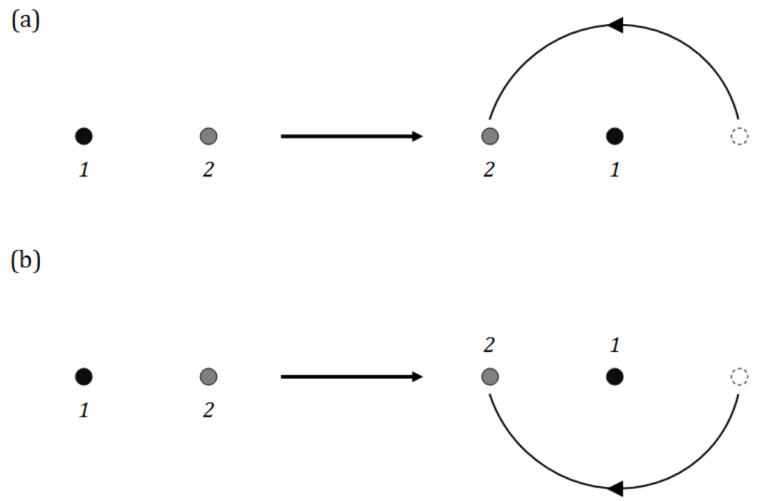

Figure 14: Exchanging two particles: (a) corresponds to $\Delta\phi = \pi$ (b) corresponds to $\Delta\phi = \pi$

It gives us

$$e^{i\nu\pi} = e^{-i\nu\pi} \implies \nu = 0, 1 \implies \psi(2,1) = \pm\psi(1,2) \tag{33}$$

These two possible phase factors ν correspond to the two only possible statistics in 3D, namely that of bosons and fermions. However, in two dimensions, there is no such equality as eq. (33), because there is no continuous deformation that takes us from path (a) to path (b). In this case, particles may neither be bosons nor fermions. They can have any statistics, and are called Anyons.

An Fibonacci Anyon model

In our model, we will be using what we call Fibonacci Anyons. They correspond to $\nu = 12/5$.

Abelian and non-Abelian Anyons

As stated previously, Anyons can be created in pairs from the vacuum, or created by splitting an Anyon into two Anyons. Let's define the notion of an anyonic charge as follows: an Anyon has a charge of 1, and the vacuum has a charge of 0. This charge is conserved inside a finite region of space. Thus, two Anyons created from the vacuum will have a total charge of 0, whereas two Anyons which where the result of splitting a parent Anyon will have a total charge of 1.

Fusion rules

We can write the process of fusion of two particles a and b into a particle c in the following algebraic manner:

$$a \circ b = c \tag{34}$$

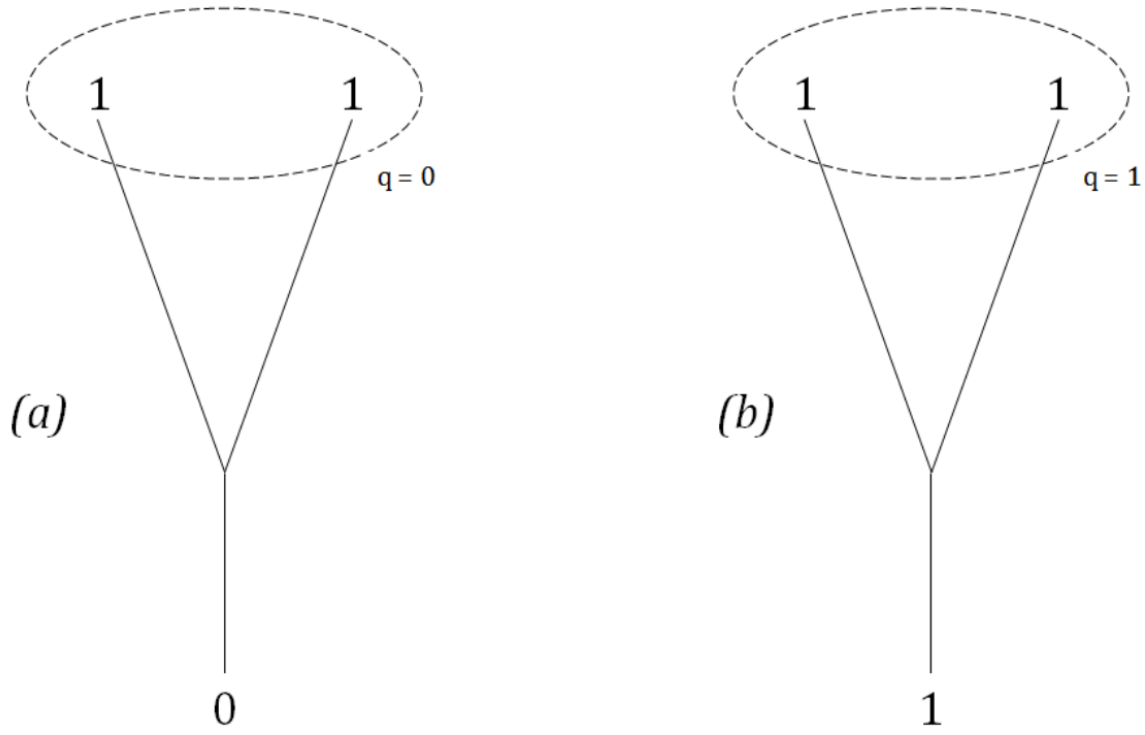

Figure 15: (a): Two Anyons with a total charge of 0 fuse to give the vacuum, (b): two Anyons with a total charge of 1 fuse to give another Anyon.

The rules as follows

$$1 \circ 0 = 1 \tag{35}$$
$$0 \circ 1 = 1 \tag{36}$$
$$0 \circ 0 = 0 \tag{37}$$
$$1 \circ 1 = 1, 0. \tag{38}$$

F and R matrices

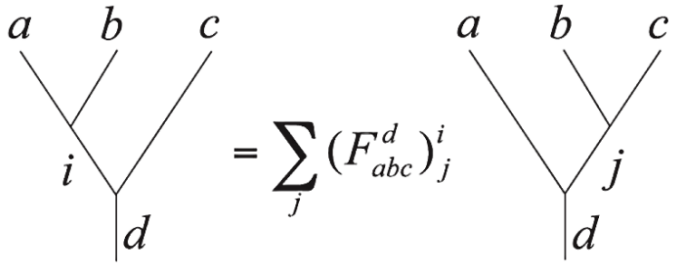

Figure 16: This figure shows how different orders of fusions are mapped to each other. a, b, c are the 3 initial Anyons, i and j are the results of the first fusion and d is the final Anyon

Mapping one order of fusion to another is done via one or multiple applications of the F-matrix as shown in fig 16. To compute the elements of the F-matrix, we can construct a consistency equation like this

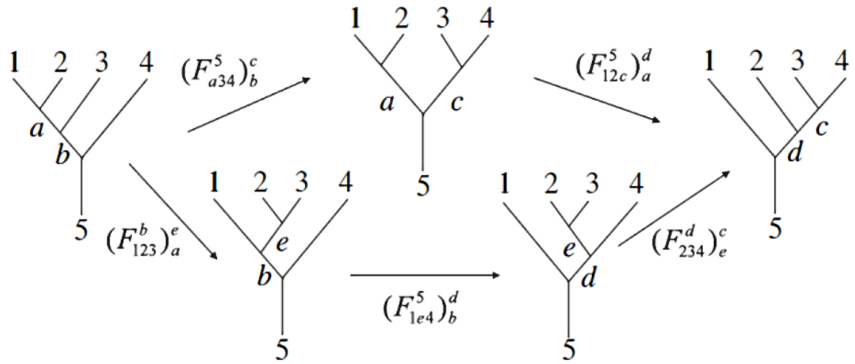

Figure 17: The Pentagon Identity: there are two ways of linking the left-to-right process to the right-to-left process.

Then we have

$$(F^d_{12c})^d_a (F^5_{a34})^c_b = \sum_e (F^d_{234})^c_e (F^5_{1e4})^d_b (F^b_{123})^e_a \tag{39}$$

By equation (39), we can find all the elements of the F-matrix, and since it has 6 indices, each one taking the values 0 or 1, there are 64 of them. For example[21],

$$(F^1_{111})^i_j = \begin{pmatrix} \frac{1}{\phi} & \frac{1}{\sqrt{\phi}} \\ \frac{1}{\sqrt{\phi}} & -\frac{1}{\phi} \end{pmatrix} \quad \text{where} \quad \phi = \text{Golden ratio} \tag{40}$$

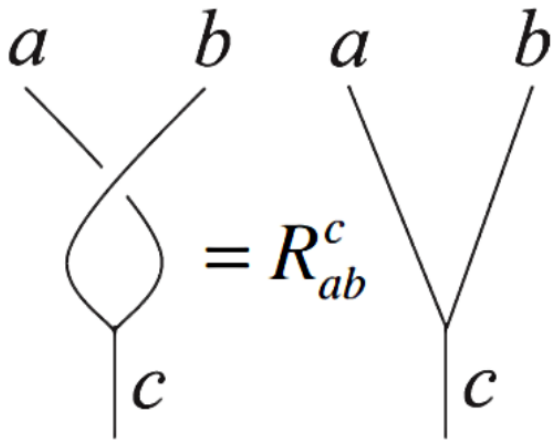

Figure 18: The R-matrix is the result of a clockwise interchanging of a and b.

Topological Quantum Computation

Similarly to the F-matrix, we can construct a consistency equation for the R-matrix. This time we call it the Hexagon Identity.

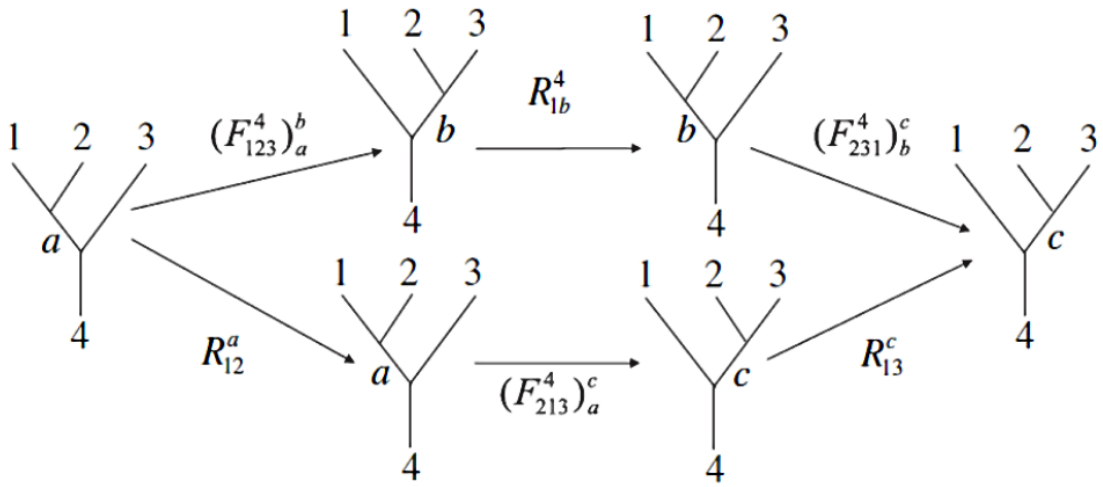

Figure 19: The Hexagon Identity is derived from this diagram.[21]

It gives

$$\sum_b (F^4_{231})^c_b R^4_{1b} (F^4_{123})^b_a = R^c_{13} (F^4_{213})^c_a R^a_{12} \tag{41}$$

For the case of two Anyons (two charges 1):

$$R_{11} = \begin{pmatrix} e^{-4\pi i/5} & 0 \\ 0 & e^{3\pi i/5} \end{pmatrix} \tag{42}$$

Braid Group

Let us consider a special operator σ_1

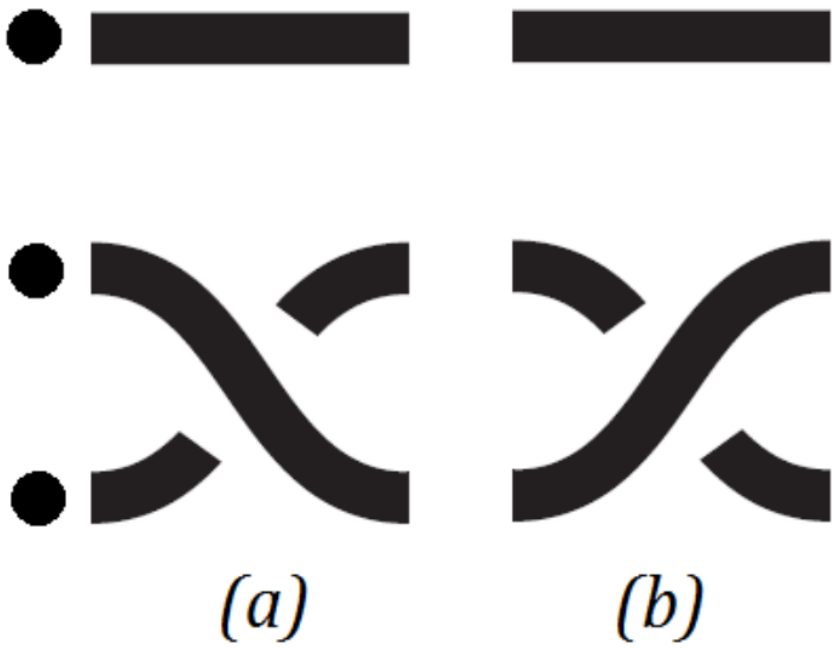

Figure 20: (a):σ_1, (b):σ_1^{-1} Time evolution is from left to right.

Define $R \equiv \sigma_1$, then find σ_2 such that

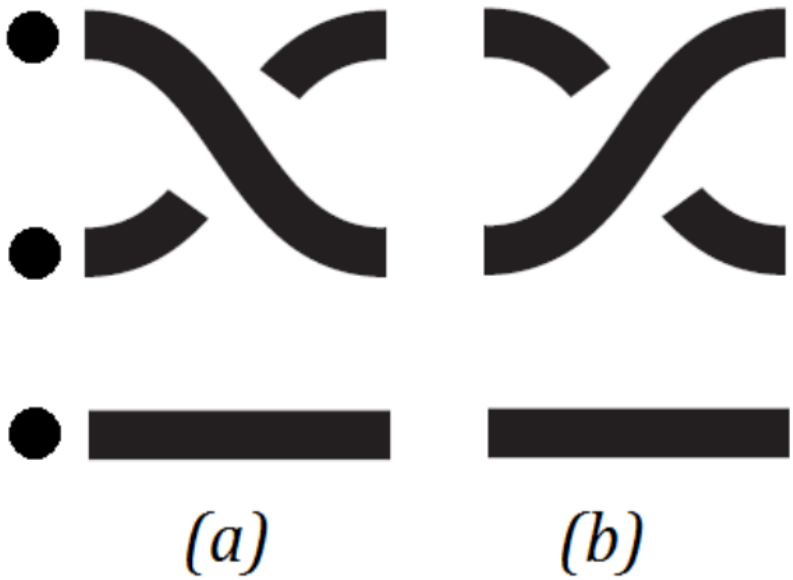

Figure 21: (a):σ_2, (b):σ_2^{-1}.Time evolution is from left to right.

σ_2 can be obtained from the successive applications of the matrices

$$\sigma_2 = F^{-1}\sigma_1 F \tag{43}$$

Matrices σ_1 and σ_2 are the generators of the Braid Group.

Topological Quantum Computation

ν can have any statistics is a crucial property for topological quantum computing ! Anyons can show a richer statistical evolution when exchanged multiple times than fermions or bosons. This is because the final phase factor will not just be ± 1 as in the bosonic and fermionic cases, instead, it can take a wide range of values depending on the statistics ν.

The reason why we are interested in the statistics of Anyons is because these particles will be used to implement qubits in a novel way.

References

[1] J. J. Sakurai and J. Napolitano, Modern Quantum Mechanics, 3rd edition. Cambridge University Press, 2021.

[2] G. Gabrielse, "The standard model's greatest triumph," Physics Today, vol. 66, no. 12, pp. 64–65, 2013. [Online]. Available: https://doi.org/10.1063/PT.3.2223

[3] S. Laporta and E. Remiddi, Physics Letters B, vol. 379, no. 1, pp. 283–291, 1996.

[4] R. Bouchendira, P. Cladé , S. Guellati-Khélifa, F. Nez, and F. Biraben, "New determination of the fine structure constant and test of the quantum electrodynamics," Physical Review Letters, vol. 106, no. 8, feb 2011.

[5] T. Aoyama, M. Hayakawa, T. Kinoshita, and M. Nio, "Tenth-order electron anomalous magnetic moment: Contribution of diagrams without closed lepton loops," Physical Review D, vol. 91, no. 3, feb 2015.

[6] D. Hanneke, S. Fogwell, and G. Gabrielse, "New measurement of the electron magnetic moment and the fine structure constant," Physical Review Letters, vol. 100, no. 12, mar 2008.

[7] J. Schwinger, "On quantum-electrodynamics and the magnetic moment of the electron," Phys. Rev., vol. 73, pp. 416–417, Feb 1948. [Online]. Available: https://link.aps.org/doi/10.1103/PhysRev.73.416

[8] T. Aoyama, M. Hayakawa, T. Kinoshita, and M. Nio, "Tenth-order qed contribution to the electron g-2 and an improved value of the fine structure constant," Physical Review Letters, vol. 109, no. 11, sep 2012.

[9] S. Peil and G. Gabrielse, "Observing the quantum limit of an electron cyclotron: Qnd measurements of quantum jumps between fock states," Phys. Rev. Lett., vol. 83, pp. 1287–1290, Aug 1999. [Online]. Available: https://link.aps.org/doi/10.1103/PhysRevLett.83.1287

[10] B. D'Urso, R. Van Handel, B. Odom, D. Hanneke, and G. Gabrielse, "Single-particle self-excited oscillator," Phys. Rev. Lett., vol. 94, p. 113002, Mar 2005. [Online]. Available: https://link.aps.org/doi/10.1103/PhysRevLett.94.113002

[11] G. Gabrielse and H. Dehmelt, "Observation of inhibited spontaneous emission," Phys. Rev. Lett., vol. 55, pp. 67–70, Jul 1985. [Online]. Available: https://link.aps.org/doi/10.1103/PhysRevLett.55.67

[12] P. Cladé, E. de Mirandes, M. Cadoret, S. Guellati-Khélifa, C. Schwob, F. m. c. Nez, L. Julien, and F. m. c. Biraben, "Determination of the fine structure constant based on bloch oscillations of ultracold atoms in a vertical optical lattice," Phys. Rev. Lett., vol. 96, p. 033001, Jan 2006. [Online]. Available: https://link.aps.org/doi/10.1103/PhysRevLett.96.033001

[13] B. N. Taylor, "Determining the avogadro constant from electrical measurements," Metrologia, vol. 31, no. 3, p. 181, jan 1994.

[14] WIKI. (2022, dec) Magnetic resonance imaging. [Online]. Available: https://en.wikipedia.org/wiki/Magnetic_resonance_imaging

[15] ——. (2022, dec) Spin–lattice relaxation.

[16] ——. (2022, dec) File:real-time mri - thorax.ogv. [Online]. Available: https://en.wikipedia.org/wiki/File:Real-time_MRI_-_Thorax.ogv

[17] ——. (2022, dec) In vivo magnetic resonance spectroscopy. [Online]. Available: https://en.wikipedia.org/wiki/In_vivo_magnetic_resonance_spectroscopy

[18] S. Fain, M. L. Schiebler, D. G. McCormack, and G. Parraga, "Imaging of lung function using hyperpolarized helium-3 magnetic resonance imaging: Review of current and emerging translational methods and applications," Journal of Magnetic Resonance Imaging, vol. 32, no. 6, pp. 1398–1408, 2010. [Online]. Available: https://onlinelibrary.wiley.com/doi/abs/10.1002/jmri.22375

[19] G. Giovannetti, A. Guerrini, and P. A. Salvadori, "Magnetic resonance spectroscopy and imaging for the study of fossils," Magnetic Resonance Imaging, vol. 34, no. 6, pp. 730–742, 2016. [Online]. Available: https://www.sciencedirect.com/science/article/pii/S0730725X16000321

[20] A. Deshmukh, "An introduction to anyons."

[21] J. K. Pachos, Introduction to Topological Quantum Computation. Cambridge University Press, 2012.